Journal of Oceanography, Vol. 56, pp. 625 to 642, 2000

Applications of the Mild-Slope Equation to Tidal Computations in the Taiwan Strait

MING-CHUNG LIN[1], WEN-JYE JUANG[2]* and TING-KUEI TSAY[3]

[1]*Department of Naval Architecture and Ocean Engineering, National Taiwan University, Taipei 106, Taiwan*
[2]*Institute of Harbor and Marine Technology, Ministry of Transportation and Communications, Wu-chi 435, Taiwan*
[3]*Department of Civil Engineering, National Taiwan University, Taipei 106, Taiwan*

(Received 14 December 1999; in revised form 26 April 2000; accepted 7 June 2000)

Employing harmonic analysis of tidal data in the Taiwan Strait, the cross-strait tidal characteristics are completely illustrated. Based on the two dimensional mild-slope equation which can be reduced to the shallow-water wave equation, a finite element model (Tsay *et al.*, 1989) is applied to investigate the characteristics of tides in the Taiwan Strait. The co-range and equi-phase charts of major tidal constituents, such as M_2, S_2, N_2, and K_1, are reproduced. Anomalous amplification of semidiurnal tides in the Taiwan Strait is verified. With rotation effects neglected and by applying a non-reflective condition on the open boundaries, the numerical results of phase-lag and co-range distributions show very good agreement with observed data for semidiurnal tides in the Taiwan Strait. Due to crude representation of the topography at two ends along the China coast, computed tidal distributions deviate from the observations. However, both computed amplitudes and phase-lags compare very well with observed data along the central half of the China coast.

Keywords:
· Standing tides,
· Taiwan Strait,
· amplification,
· resonance,
· wave trapped,
· local radiation condition.

1. Introduction

The Taiwan Strait is a slender channel extending roughly 600 km longitudinally and no more than 150 km across the narrowest span. It is surrounded by the East China Sea to the north, the main island of Taiwan to the east, the Bashi Channel and the South China Sea to the south, and the east coast of China to the west, Fig. 1. There are dense tidal stations distributed around the cross-strait coasts. The Taiwan Strait with an averaged water depth of less than 80 m is a much shallower and flatter connection between the East and the South China Seas, and it eventually connects to the West Pacific Ocean. It situates just inside the brink of the Asia continental shelf with the Continent Slope and the Kao-ping Slope located respectively at the northeast and southwest rims, Fig. 2. The Taiwan Bank with most of the water depths less than 30 m situates right at strait's south rim.

The tides of the Taiwan Strait are of considerable importance for operation of ports and cities located around the Strait. The tidal range reaches more than 5 m at the central part and it is relatively small at both ends (less than 1.3 m). In the past several decades, anomalous amplification of tides along the west coast of Taiwan had received great attentions from both coastal and oceanographical researchers. Based on speculations of shoaling and diffraction effects, most researchers inferred that the anomalous amplification of tides resulted from encountering effects of two opposite tidal waves. But the question why the tides are unusually large in the central part of the Taiwan Strait has not been clarified. A recent research regarding to tidal distributions around coast of Taiwan has been reported (Lin *et al.*, 2000). In this paper, tidal distribution in the Taiwan Strait including both coasts of Taiwan and China will be emphasized.

To understand the amplification mechanisms and to explore various characteristics of tides in the Taiwan Strait, accurate computational models are required. For depth-varying topography, a two-dimensional linear depth-integrated wave model (Tsay, 1991) which extends the mild-slope equation (Berkhoff, 1972; Smith and Sprinks, 1975) can be applied to determine the motion of monochromatically tidal waves propagating in a basin with moderate bottom slope. The advantage of this equation is applicable not only to a broad range of wave fre-

* Corresponding author. E-mail: wjjuang@ms1.hinet.net

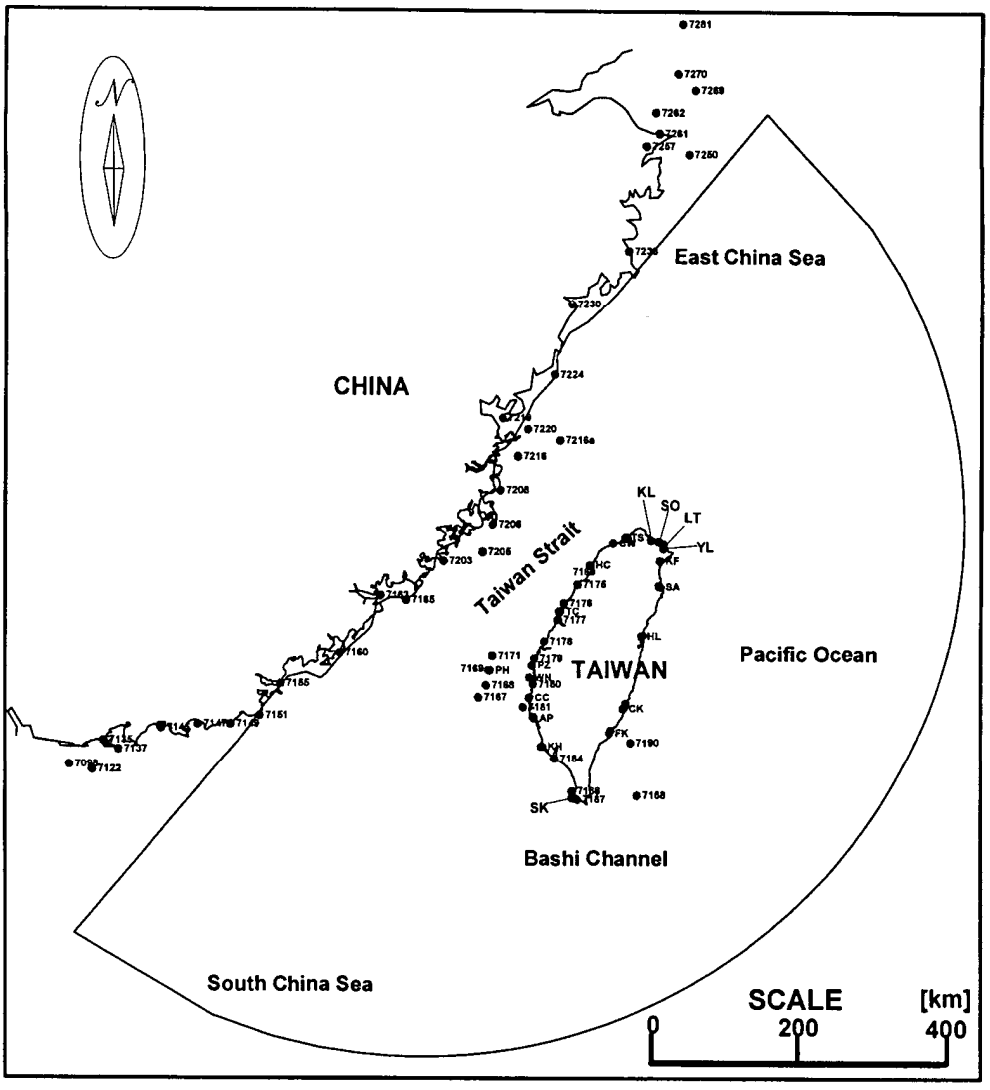

Fig. 1. Locations of tidal stations on both coastal boundaries of the Taiwan Strait. The quasi semi-circle defines the domain of computation.

quencies but also the moderate topography effects (Mei, 1983; Tsay, 1991). Moreover, Booij (1983) has discussed that acceptable results can be obtained by the mild-slope equation even though the bottom slope is not moderate. Kirby (1986) has extended the mild-slope equation to account for a fast-varying topography. By introducing the horizontal pseudo fluxes, Copeland (1985) has demonstrated that the mild-slope equation can be transformed into forms similar to the shallow-water wave equation. Madsen and Larsen (1987) developed an efficient Alternate-Direction-Implicit finite-difference algorithm to find the stationary solution by which large model areas can be handled with a relatively small amount of computational effort. A numerical model of the mild-slope equation is recently employed in tidal computations (Lin *et al.*, 2000). This two-dimensional model is of an energy-conserving form. Other three-dimensional models have also been proposed to investigate tidal behavior in this area (Liu, 1984; Guo and Yanagi, 1998).

In this paper, tidal characteristics along east and west coasts of the Taiwan Strait are discussed in the following section. In Section 3, the mild-slope model equation for shallow water is introduced. The neglect of effects of Coriolis force in present study is justified. In Section 4, a brief description of the finite element model is included for completeness and local radiation (non-reflective) conditions applied to the open boundaries are introduced. Some descriptions are given in Section 5 to the computa-

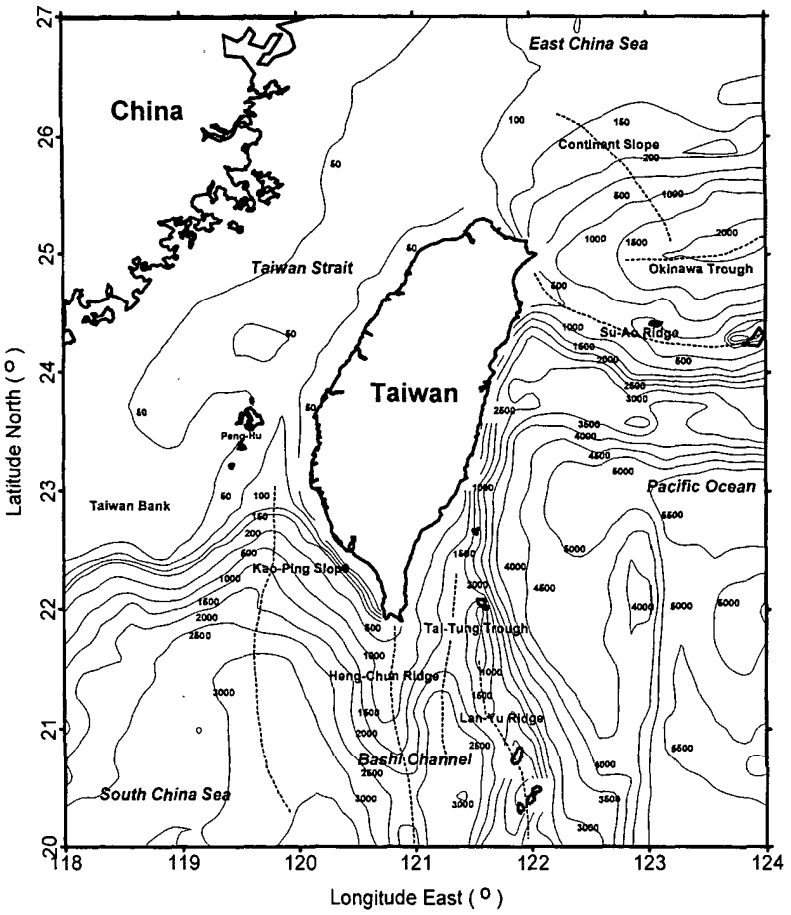

Fig. 2. Topography in the Taiwan Strait and the surroundings of Taiwan. Water depth is in meters. Dotted lines represent the position of shelf slope, ridges, and troughs.

tional details as well as the data analysis. A conceptual oscillating configuration similar to tidal appearance in the Taiwan Strait is proposed in Section 6. The co-range and equi-phase charts also are demonstrated. Finally, verifications of model results compared with observed data are presented. Conclusions are summarized in the last section.

2. Characteristics of Tides and Topography

There are many tidal stations distributed on both coastal sides of the Taiwan Strait (Fig. 1). However, tides in the Taiwan Strait especially along to the coasts of Taiwan and China, are rarely reported in the open literature. Distributions of amplitudes and phase-lags of main tidal constituents such as M_2, S_2, N_2, K_1, O_1, and P_1 along the coasts of Taiwan and China, after applying the Simple Harmonic Analysis Method (SHAM) to tidal measurements are listed in Tables 1 and 2, respectively. Relevant tidal constituent data are shown graphically in Figs. 3 and 4, respectively. In the tables and figures, tidal stations represented by the abbreviation of station location are established by the Central Weather Bureau, Taiwan (CWBT), for long-term measurements. The others, expressed only by the number, are cited from the Admiralty Tide Tables (UKHO, 1997). Comparing the constituent harmonic constants of Taiwan, shown in Table 1 and Fig. 3, it is noted that the harmonic constants obtained from CWBT and UKHO are in good accordance. Based on these tidal constituent harmonic constants, anomalous amplification of semidiurnal tides along the west coast of Taiwan can be noted.

The distributions of tidal range appear to be almost symmetric with respect to the central part of the Taiwan Strait, Figs. 3(a) and 4(a). Furthermore, the tidal ranges along the coast of China are larger than along the west coast of Taiwan. Along the east flank of the Taiwan Strait, the maximum tidal range occurs almost at the central west coast of Taiwan and its range decreases toward both northwest and southwest ends. The average tidal ranges on central west coast of Taiwan are about four times of those

Table 1. Amplitudes, and phase-lags of main tidal constituents at tidal stations around the main island of Taiwan.

No.	Place or station	Lat. N D°M′	Long. E D°M′	M.L. Z_0 (m)	Harmonic constants											
					M_2		S_2		N_2		K_1		O_1		P_1	
					g^0	H.m	g^0	H.m	g^0	H.m	g^0	H.m	g^0	H.m	g^0	H.m
SA	Su-ao Kang	24°35′	121°52′	0.00	169	0.418	201	0.181	158	0.082	226	0.197	191	0.171	223	0.065
7196	Su-ao Kang	24°35′	121°52′	0.99	169	0.44	203	0.19			225	0.18	191	0.18		
KF	Geng-fang	24°54′	121°52′	0.00	187	0.364	215	0.148	178	0.077	220	0.194	187	0.160	218	0.061
YL	Yan-liao	25°03′	121°55′	0.00	198	0.206	216	0.106	190	0.051	220	0.191	187	0.157	216	0.062
LT	Long-dong	25°06′	121°55′	0.00	209	0.225	230	0.113	198	0.056	222	0.199	188	0.165	218	0.066
SO	Shen-ao	25°08′	121°51′	0.00	251	0.175	246	0.069	224	0.048	225	0.190	191	0.158	222	0.063
KL	Kee-lung	25°09′	121°45′	0.00	278	0.219	281	0.056	246	0.056	228	0.187	194	0.156	225	0.062
7198	Chi-lung	25°09′	121°45′	0.58	283	0.19	281	0.05			230	0.19	197	0.15		
TS	Tan-shui	25°11′	121°24′	0.00	313	1.03	351	0.289	286	0.192	244	0.217	208	0.183	241	0.069
7173	Tan-shui Kang	25°11′	121°26′	1.58	319	1.00	359	0.31			248	0.20	207	0.17		
CW	Chu-wei	25°07′	121°14′	0.00	316	1.196	355	0.341	289	0.221	248	0.224	211	0.189	244	0.069
HC	Hsin-chu	24°51′	120°55′	0.00	319	1.610	360	0.467	293	0.291	257	0.235	218	0.199	253	0.073
7175	Hou-lung	24°37′	120°45′	2.5	323	1.63	366	0.50			264	0.20	213	0.17		
7176	Ta-an Kang	24°23′	120°34′	2.66	323	1.72	366	0.51			261	0.22	226	0.21		
TC	Tai-chung	24°17′	120°31′	0.00	324	1.719	369	0.486	299	0.296	268	0.252	229	0.206	265	0.087
7176a	T'ai-chung Kang	24°17′	120°30′	2.65	317	1.70	370	0.46			262	0.22	221	0.19		
7177	T'u-ko-k'u	24°11′	120°29′	2.18	327	1.48	376	0.37			268	0.18	222	0.15		
7178	Fong-yuang	23°55′	120°18′	2.17	331	1.43	379	0.32			273	0.22	235	0.20		
7171	Chi-pei Tao	23°44′	119°36′	2.1	332	1.21	395	0.30			277	0.23	237	0.22		
7179	T'ai-hsi	23°42′	120°10′	1.73	331	1.14	379	0.25			273	0.18	235	0.16		
PZ	Po-Zi-Liao	23°37′	120°08′	0.00	318	1.051	364	0.277	285	0.186	282	0.230	230	0.202	284	0.061
PH	Peng-hu	23°33′	119°34′	0.00	324	0.892	373	0.223	298	0.163	280	0.249	237	0.216	275	0.081
7169	Ma-Kung Kang	23°33′	119°33′	1.6	326	0.87	375	0.23			278	0.25	236	0.21		
WN	Wen-kang	23°28′	120°06′	0.00	310	0.693	354	0.163	286	0.128	282	0.217	239	0.191	280	0.065
TG	Dong-shi	23°27′	120°08′	0.00	314	0.654	360	0.15	288	0.120	285	0.208	243	0.182	281	0.062
7180	Pu-tai	23°23′	120°09′	1.13	311	0.60	364	0.14			278	0.2	237	0.19		

No.	Place or station	Lat. N D°M′	Long. E D°M′	M.L. Z_0 (m)	Harmonic constants											
					M_2		S_2		N_2		K_1		O_1		P_1	
					g^0	H.m	g^0	H.m	g^0	H.m	g^0	H.m	g^0	H.m	g^0	H.m
7168	Chiang-chun Kang-tao	23°22′	119°31′	1.2	324	0.60	376	0.12			277	0.22	238	0.2		
CC	Chiang-chun	23°13′	120°06′	0.00	313	0.463	351	0.098	282	0.077	287	0.187	244	0.161	286	0.059
7167	Ch'i-mei Yu	23°13′	119°25′	1.2	329	0.55	379	0.12			285	0.24	235	0.21		
7181	Kuo-sheng Kang	23°06′	120°01′	0.70	295	0.29	330	0.04			278	0.19	236	0.18		
AP	An-ping	22°58′	120°10′	0.00	258	0.236	268	0.059	238	0.052	277	0.181	234	0.165	268	0.059
7182	An-P'ing Kang	22°59′	120°09′	0.68	263	0.25	278	0.06			299	0.2	244	0.17		
KH	Kao-hsiung	22°37′	120°17′	0.00	218	0.169	223	0.066	193	0.043	283	0.162	234	0.154	279	0.062
7183	Kao-hsiung Kang	22°37′	120°16′	0.52	236	0.15	248	0.06			294	0.16	249	0.15		
7184	Tung-kang	22°28′	120°27′	0.6	229	0.20	235	0.07			298	0.2	246	0.17		
7186	Ch'e-ch'eng	22°04′	120°41′	0.69	200	0.20	223	0.10			282	0.22	237	0.17		
SK	Xun-Guang-Zui	21°59′	120°41′	0.00	194	0.206	216	0.089	181	0.042	277	0.222	236	0.188	273	0.068
7187	Ta-Pan-Lieh	21°58′	120°45′	0.78	188	0.26	214	0.11			262	0.23	224	0.18		
7188	Lan Yu	22°01′	121°33′	0.88	174	0.45	218	0.20			244	0.11	208	0.12		
7190	Lu Tao	22°40′	121°28′	0.86	165	0.42	213	0.19			232	0.12	192	0.13		
FK	Fu-kang	22°47′	121°11′	0.00	172	0.430	203	0.170	161	0.075	231	0.167	196	0.161	224	0.051
7191	Fu-kang	22°49′	121°12′	0.93	167	0.43	193	0.18			233	0.16	194	0.16		
CK	Cheng-kuang	23°06′	121°22′	0.00	175	0.426	203	0.200	157	0.095	221	0.172	190	0.150	218	0.057
7192	Ch'eng-kuang	23°09′	121°24′	1.01	166	0.51	204	0.21			220	0.16	191	0.13		
HL	Hua-lian	23°59′	121°37′	0.00	175	0.426	204	0.192	154	0.079	220	0.147	195	0.137	213	0.049
SA	Su-ao Kang	24°36′	121°51′	0.00	169	0.418	201	0.181	158	0.082	226	0.197	191	0.171	223	0.065
7196	Su-ao Kang	24°35′	121°52′	0.99	169	0.44	203	0.19			225	0.18	191	0.18		

Table 2. Amplitudes, and phase-lags of main tidal constituents at tidal stations along part of the east coast of China.

No.	Place	Lat. N D°M′	Long. E D°M′	M.L. Z_0 (m)	Harmonic constants								S.W. corrections			
					M_2		S_2		K_1		O_1		1/4 diurnal		1/6 diurnal	
					g^0	H.m	g^0	H.m	g^0	H.m	g^0	H.m	f_4	F_4	f_6	F_6
7281	Sheshan	31°25′	122°14′	2.29	309	1.25	005	0.52	184	0.16	123	0.13				
7270	Dajishan	30°49′	122°10′	2.5	288	1.3	342	0.5	192	0.3	145	0.2				
7269	Baijieshan	30°37′	122°25′	2.5	286	1.2	330	0.5	198	0.3	156	0.2				
7262	Yuxingnao	30°21′	121°51′	2.26	341	1.12	023	0.43	213	0.38	171	0.19	224	0.059		
7261	Xihu Men	30°06′	121°54′	2.1	298	1.1	340	0.4	211	0.3	167	0.2				
7257	Zhenhai	29°57′	121°43′	2.07	359	0.74	023	0.29	221	0.3	198	0.23				
7250	Ch'ing-tzu Men	29°51′	122°19′	2.4	265	1.2	308	0.5	215	0.3	170	0.2				
7236	Haimen Gang	28°41′	121°27′	w	275	1.81	332	0.7	249	0.22	188	0.13	273	0.047	195	0.004
7230	Wenzhou Gang	28°02′	120°39′	w	316	1.66	014	0.53	259	0.22	212	0.16	297	0.08	185	0.009
7224	Shacheng Gang	27°10′	120°25′	3.4	272	2.0	319	0.7	232	0.3	195	0.2				
7219	Sando Ao	26°38′	119°42′	4.27	300	2.57	346	0.79	246	0.35	202	0.24	103	0.023		
7220	Xiyang Dao	26°30′	120°03′	3.5	290	2.1	337	0.7	232	0.3	200	0.2				
7216a	Dongyin Dao	26°22′	120°30′	2.78	332	1.7	032	0.54	245	0.30	221	0.24				
7216	Mazu Dao	26°10′	119°55′	3.7	293	2.3	340	0.8	234	0.3	205	0.2				
7208	Dongluo Liedao	25°45′	119°41′	3.6	308	2.1	356	0.7	234	0.3	218	0.2				
7206	Ren Yu	25°20′	119°35′	3.57	318	2.06	005	0.68	236	0.28	222	0.22	285	0.006		
7205	Wuqiu Yu	25°00′	119°27′	3.24	340	2.13	018	0.56	257	0.28	245	0.27				
7203	Chongwu	24°53′	118°55′	3.51	359	2.0	017	0.6	246	0.3	228	0.2				
7163	Xiamen Gang	24°27′	118°04′	3.28	352	1.84	043	0.54	281	0.34	238	0.28	006	0.027	058	0.011
7165	Liaoluo Wan	24°24′	118°25′	2.69	090	1.6	125	0.54	139	0.31	122	0.24				
7160	Dongshan	23°44′	117°32′	2.16	007	1.05	059	0.31	289	0.33	238	0.25	088	0.030		
7169	Ma-Kung Kang	23°33′	119°33′	1.60	326	0.87	015	0.23	278	0.25	236	0.21	359	0.099		
7155	Shantou Gang	23°20′	116°45′	1.37	021	0.42	094	0.10	294	0.30	249	0.24				
7151	Shibeishan Jiao	22°56′	116°29′	1.1	000	0.2	050	0.1	293	0.4	247	0.2				
7149	Jiazi Jiao	22°49′	116°06′	0.89	315	0.2	000	0.1	292	0.4	247	0.2				
7147	Jieshi Wan	22°48′	115°40′	1.22	248	0.22	276	0.09	291	0.38	246	0.23				
7145	Honghai Wan	22°44′	115°11′	1.1	250	0.3	277	0.1	293	0.4	247	0.2				
7135	Ping Chau	22°33′	114°26′	1.3	268	0.4	300	0.2	305	0.4	247	0.3				
7137	Tuoning liedao	22°27′	114°38′	1.2	260	0.3	290	0.2	294	0.3	246	0.3				
7098	Chi Ma Wan	22°14′	114°00′	1.35	268	0.42	299	0.17	299	0.36	251	0.29				
7122	Waglan island	22°11′	114°18′	1.43	265	0.34	296	0.14	301	0.34	252	0.28				

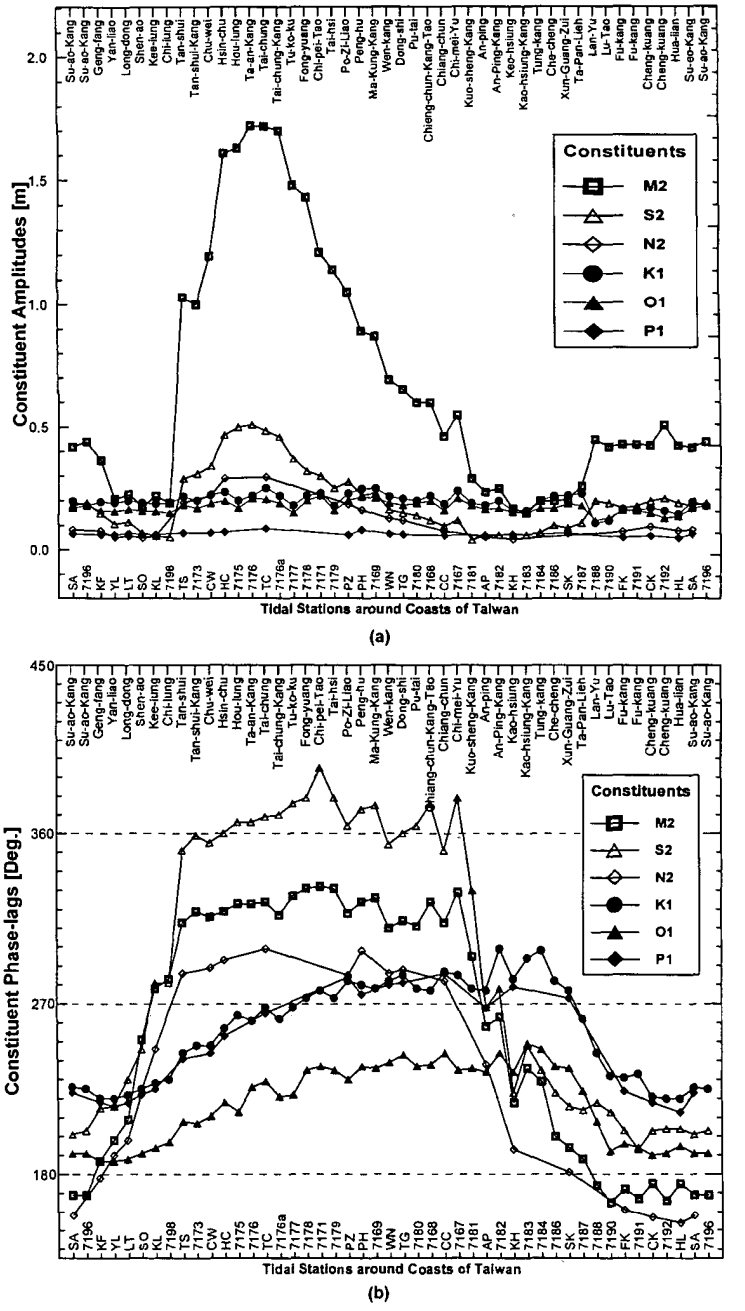

Fig. 3. Distributions of amplitudes, (a) and phase-lags, (b) of measured tidal constituents around the coast of Taiwan.

on the east coast and they reach almost seven times of those of the northeast and southwest coasts. In particular, even though stations Kee-lung (KL) and Kao-hsiung (KH) are about 400 km apart, the tidal ranges at these two stations are almost the same.

The difference of phase-lag/epoch (Schureman, 1988) between two adjacent stations is used to indicate the time that tides take to propagate from one station to another. From Figs. 3(b) and 4(b), it is noted that the phase-lag distributions of diurnal and semidiurnal constituents both appear nearly symmetrical along the coast of both sides. Around the coast of Taiwan, the phase-lags of the semidiurnal constituents between station Tan-shui (TS) and station Chiang-chun (CC) are approximately equal to a constant value. The difference of phase-lags of diurnal constituents between stations Su-ao (SA) and CC

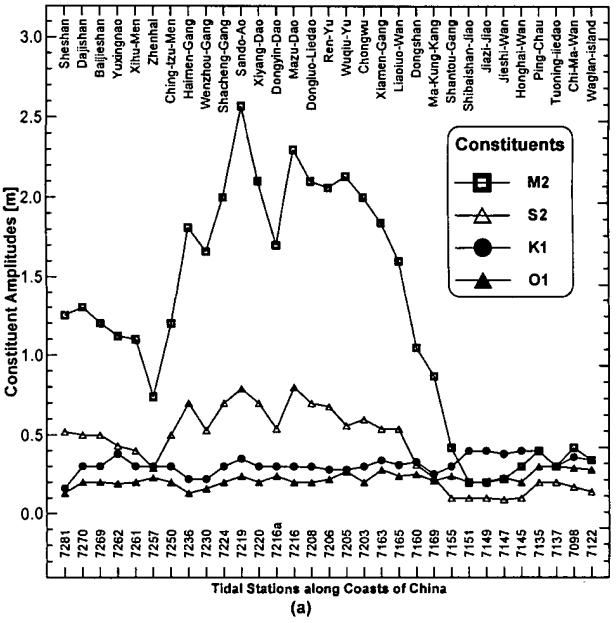

Fig. 4. Distributions of amplitudes, (a) and phase-lags, (b) of measured tidal constituents along part of the east coast of China.

is about 45 degrees. It takes approximately 3 hours for diurnal tides to propagate from northeast to southwest coast. For semidiurnal tides, difference of phase-lags between central west station Tai-chung (TC) and station SA is about 150 degrees. However, sharp variations are observed around the northeast coast from station Su-ao (SA) to TS and around the southwest coast from station CC to KH, respectively. It takes 5 hours for semidiurnal tides to

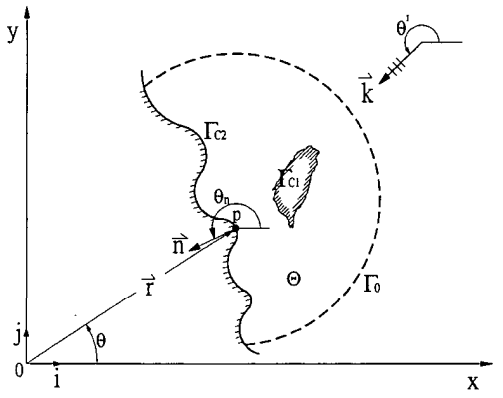

Fig. 5. Schematic definition of irregular coastlines, boundaries, and incident waves on the Cartesian and polar coordinates.

propagate between these two stations. Along the north coast from station SA to station TS, it takes 4 hours for semidiurnal tides to propagate a distance of less than 100 km. Similar phase-lag difference is also found for a distance slightly longer than 100 km along the south coast from station Xun-guang-Zui (SK), the southernmost station of Taiwan, to station CC. It is worth pointing out that the phase-lags distributed around the east coast of Taiwan are generally less than that of the west coast. Similar phase-lag distribution is also found along the China coast. The tides appear to reach the east coast of Taiwan first and then diffract into the Taiwan Strait by passing through the northeast and southwest ends separately, and finally encounter with each other near the central basin in the Strait.

The regional bathymetry and topography can substantially affect the characteristics of tides. Extracting a topographical profile from Fig. 2 with a distance of 50 km off the coasts around Taiwan, it is interesting to note that there is a shelf-like topography with the length about 650 km extending from northwest station Long-dong (LT) to southwest station An-ping (AP). It is further observed that the station Shen-ao (SO) at northeast coast of Taiwan, which has relatively small semidiurnal amplitude, is situated near the edge of the shelf. The station KH at southwest coast, which also has relatively small semidiurnal amplitude, is located right outside of the shelf and is situated on the shelf slope. Moreover, the station TC on central west coast with maximum amplitude of semidiurnal constituents is roughly located at the middle section of the shelf.

3. Hydrodynamic Model Equations

Because of the complex characteristics of tides and topography in the Taiwan Strait, a numerical model in-

cluding topographical and Coriolis effects may be needed. For a computation domain containing the Taiwan Strait with mean latitude of 24°N and with the latitude span of approximated 3 degrees only, it is reasonable to assume a constant Coriolis parameter in the model formulation.

To take the topographical effects into account, a two-dimensional depth-integrated linear shallow-water wave equation with rotation is adopted (Longuet-Higgins, 1968, 1969; Tsay, 1991)

$$\nabla\cdot\left(gh\nabla\varsigma\right)+\sigma^2\left(1-f^2/\sigma^2\right)\varsigma=0; \tag{1}$$

$$\begin{Bmatrix}u\\v\end{Bmatrix}=\frac{-g}{\sigma^2\left(1-f^2/\sigma^2\right)}\begin{bmatrix}i\sigma & -f\\ f & i\sigma\end{bmatrix}\begin{Bmatrix}\dfrac{\partial\varsigma}{\partial x}\\[2ex]\dfrac{\partial\varsigma}{\partial y}\end{Bmatrix}, \tag{2}$$

subject to the assumption of $|\nabla h| = O(h/L) << 1$, where $\nabla = (\partial/\partial x, \partial/\partial y)$ denotes the space gradient operator on the horizontal right-hand Cartesian coordinate (x,y); h the water depth; L the characteristic wave length. ς denotes free surface displacement of tidal constituent with intrinsic frequency, $\sigma = 2\pi/T$; T is the harmonic period, $f = 2\Omega\sin\phi$ denotes the Coriolis parameter; $\Omega = 7.3 \times 10^{-1}S^{-1}$ the rotating angular frequency of earth; ϕ the latitude, u and v the corresponding flow velocities, g the gravitational acceleration, and $i = \sqrt{-1}$ denotes the imaginary number.

Because the semidiurnal constituents are dominant in the Taiwan Strait, the Coriolis parameter may be neglected when f^2 is small compared with σ^2 in Eq. (1). To justify this fact, let T_{M_2} = 12.4206 hr represents the period of semidiurnal constituent, the characteristic latitude of the Taiwan Strait is 24°N and the period of earth rotation is T_Ω = 24 hr, the term

$$f^2/\sigma^2 = 4\sin^2\phi\left(T_{M_2}/T_\Omega\right)^2 \approx 0.1772. \tag{3}$$

Consequently, neglecting the f^2/σ^2 term in Eq. (1) is a reasonable simplification for semidiurnal tidal computation. In the absence of rotation effects and with the long wave approximation ($h/L < 1/20$, or $kh << 1$), Eq. (1) can be further reduced to:

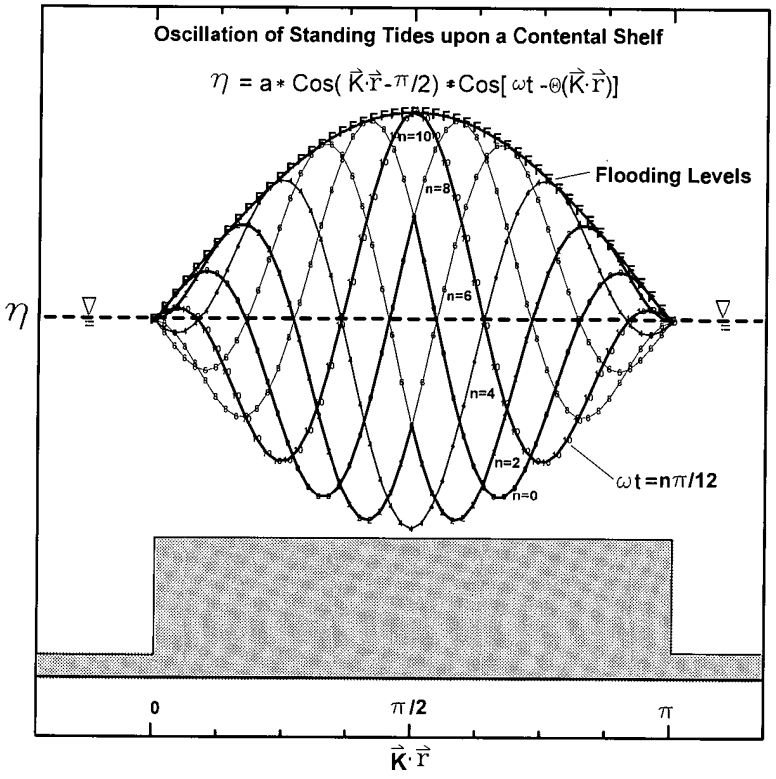

Fig. 6. Conceptual configuration of standing tides oscillating on an idealized topographical shelf.

$$\nabla \cdot (gh\nabla\varsigma) + \sigma^2\varsigma = 0. \tag{4}$$

Without the Coriolis parameter, Eq. (4) is the form of long-wave approximation to the linear mild-slope equation (Berkhoff, 1972; Chen and Mei, 1974; Smith and Sprinks, 1975; Booij, 1983; Kirby, 1986; Tsay, 1991). It has been widely applied to evaluate the combined effects of reflection, refraction and diffraction for waves over varying topography. To capture the predominant characteristics of semidiurnal constituents in the Taiwan Strait, Eq. (4) is adopted in present study.

4. A Finite-Element Numerical Model

In order to calculate the tidal distributions within the Taiwan Strait, the computational domain is chosen to consist of some coastlines of China and a nearly half circle enclosing the main island of Taiwan (Fig. 1). It is noted that both opposite ends of the China coastline deviate from the real ones. With the coordinate systems defined in Fig. 5, the incident tidal waves, ς^I, of specific constituent with wave number, k_0, in general can be expressed as

$$\varsigma^I = A_0 e^{ik_0 r\cos(\theta-\theta^I)}, \tag{5}$$

where A_0 is amplitude, r is the magnitude of position vector, θ^I is the incident angle measured from positive x axis in counterclockwise sense. By using the finite element method with linear triangular isoparametric elements to solve Eq. (4), the computational domain, Θ, must first be discretized, of which Γ_O denotes the open-sea artificial boundary, Γ_{C_1} and Γ_{C_2} denotes the coastline.

In the absence of Coriolis effects, and assuming either zero-depth, $h = 0$, or impermeable, $\partial\varsigma/\partial\vec{n} = 0$ at the coast, a combined natural condition (Tsay *et al.*, 1989) is applied:

$$h\frac{\partial\varsigma}{\partial\vec{n}} = 0, \tag{6}$$

where $\vec{n}$ denotes the outward normal unit vector along the coastal boundaries. On the open-sea artificial boundary, the free surface displacements are expressed as linear superposition of ς^I and ς^S

$$\varsigma = \varsigma^I + \varsigma^S, \tag{7}$$

where ς^S represents the scattered tidal waves and satisfies the local radiation condition along Γ_O (Chapman, 1985; Tsay *et al.*, 1989):

$$\frac{\partial\varsigma^S}{\partial\vec{n}} - ik\varsigma^S = 0, \tag{8}$$

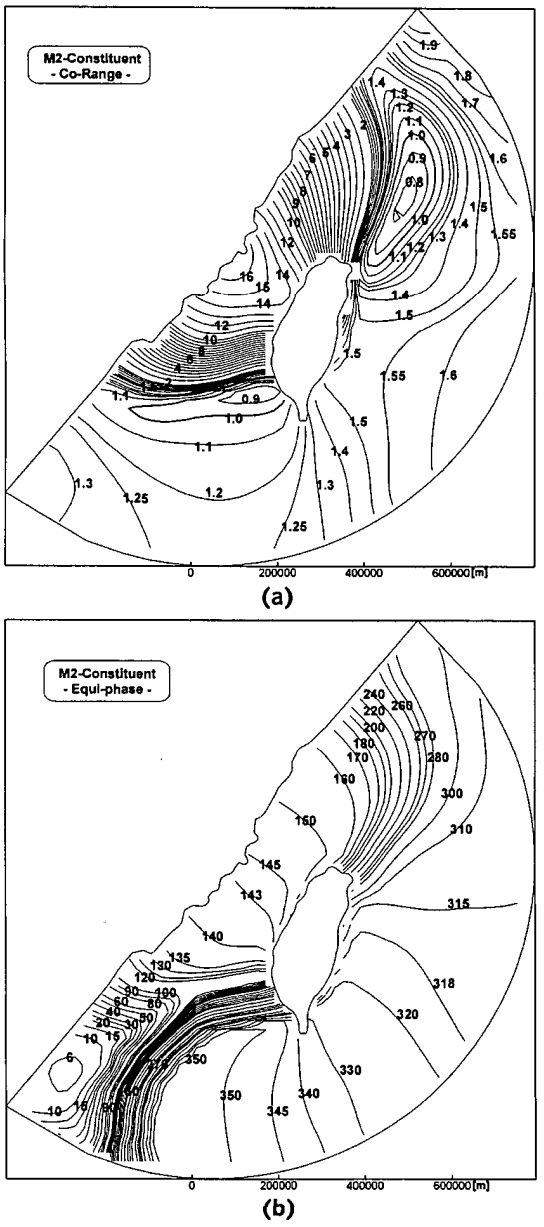

Fig. 7. Comparisons of computed amplitudes and phase-lags of M_2 constituent with incident angle of 180°. (a) and (b): computed co-range chart and equi-phase chart, (c) and (d): around the coast of Taiwan, (e) and (f): along part of the east coast of China.

where k the local wave number, since the water depths do not always remain constant along the open-sea boundary. Equation (8) is valid when the location of open boundary is at least one and half times of the incident wavelength away from the scatter (Chen and Tsay, 1990). The location of open boundary in present configuration is not suf-

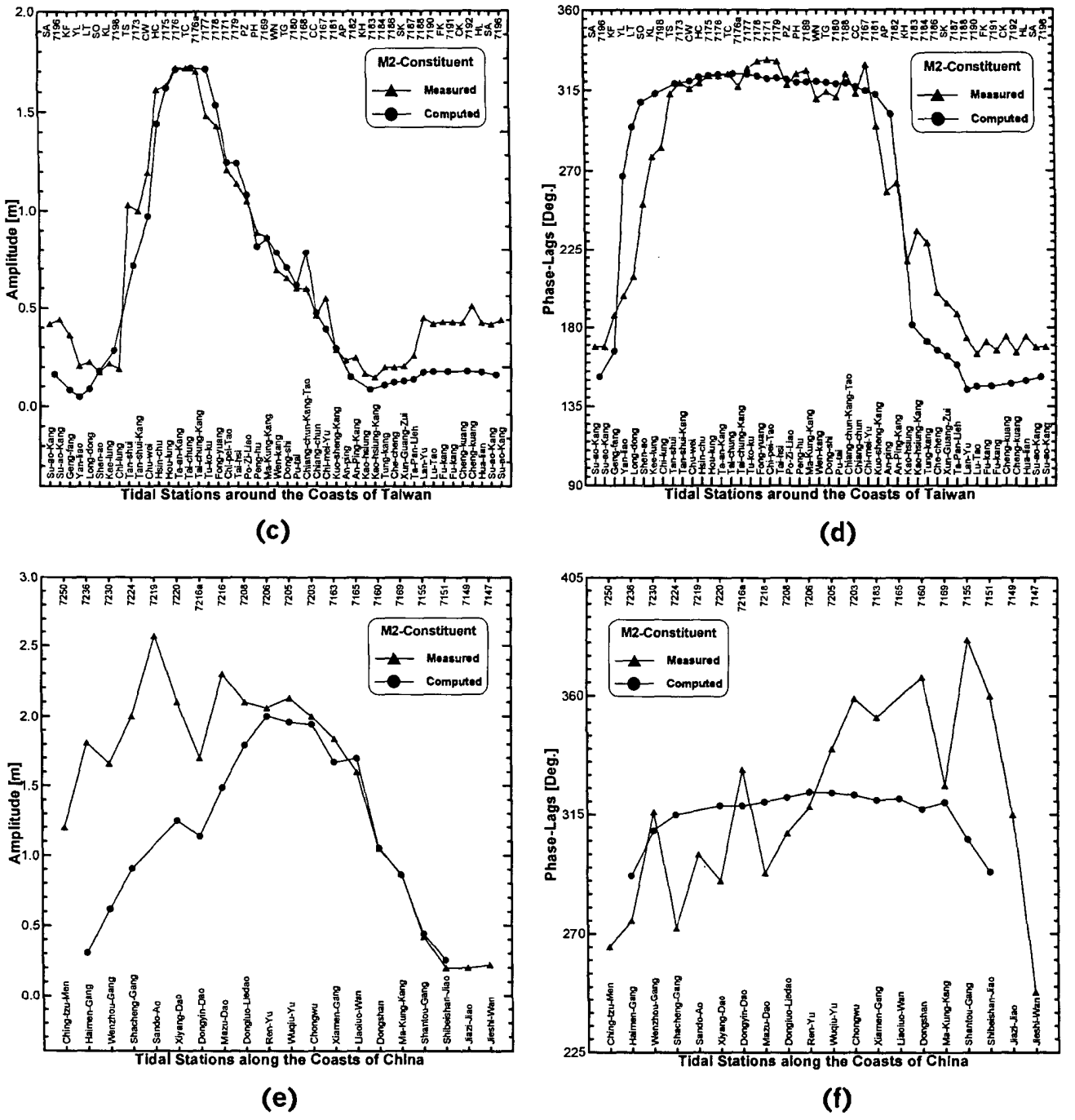

Fig. 7. (continued).

ficiently far away from the scatter for long period waves. Nevertheless, Eq. (8) is commonly used to regulate the scattered waves passing normal through the artificial open boundary (Chapman, 1985).

On constructing the finite element model, Eq. (4) can be reformulated in an integral form by Galerkin method as:

$$\iint_{\Theta}\left[\nabla W\cdot(gh\nabla\varsigma)-\sigma^2 ghW\varsigma\right]dA$$
$$-\oint_{\Gamma_0} Wgh\left[ik\varsigma\cos(\theta_n-\theta)+\frac{1}{r}\frac{\partial\varsigma}{\partial\theta}\sin(\theta_n-\theta)\right]dl$$
$$=\oint_{\Gamma_0} Wigh\cos(\theta_n-\theta)\left[k-k_0\cos(\theta-\theta^I)\right]\varsigma^I dl, \qquad (9)$$

where W is shape function of linear triangular isoparametric elements. After integrating and assembling all the elements by Eq. (9), a linear matrix equation is obtained (Tsay *et al.*, 1989; Chen and Tsay, 1990):

$$[M]\{\varsigma\} = \{F\}, \tag{10}$$

where $[M]$ is an asymmetrical stiffness matrix due to the application of local boundary condition, and $\{F\}$ the forcing matrix mainly induced by incident waves. $\{\varsigma\}$ can be solved directly by using the Gaussian elimination method. It is noted that matrix $[M]$ and $\{F\}$ have complex constants, so $\{\varsigma\}$ is a complex vector too. Thus, displacement of free surface and corresponding flow velocities, by Eq. (2), can further be expressed in terms of phase angle and amplitude by using Euler's formula.

5. Numerical Computations

For numerical computations, water depths in the computational domain (Fig. 1) are interpolated from bathymetry map published by Naval Hydrographic Office, Taiwan, in 1991. There are in total 17,582 triangular elements and 8,940 nodes generated for computation. The maximum band-width of matrix $[M]$ in Eq. (10) is not more than 150 due to the fact that the grids are structured ones. The size of each element, dl, is fine enough to satisfy the general rule of thumb in grid resolution, namely, dl is less than one-tenth of the wavelength. With such a large computation domain, only about seven minutes are needed on a Pentium II 400 Mhz CPU to execute a specific tidal constituent computation.

Instead of setting Dirichlet conditions on the open-sea boundary as in traditional transient tidal computations (Wang, 1982; Liu, 1984; Cartwright, 1990; Zahel, 1991; Lynch and Naimie, 1993; Egbert *et al.*, 1994; Le Provost *et al.*, 1994; Wagner *et al.*, 1994; Yanagi *et al.*, 1997; Guo and Yanagi, 1998), only the angle and amplitude of incident tidal waves are needed in present numerical computations. Preceding the computations, the phases of incident tidal wave can be determined non-uniformly according to Eq. (5) along the semicircle open boundary. After experimenting for the best-fit results, it is found that the constituent tidal waves with incident angle, θ^I, of 180° give the best results and are shown in present study.

Without losing generalities of linear model, the amplitude of incident tidal waves is assumed to be one unit. For comparisons with measurements, both the calculated amplitudes and phase angles are calibrated to the constituent harmonic constants of station TC, which has maximum constituent amplitudes on the west coast of Taiwan. A scaling factor of amplitude and a phase difference with respect to station TC between calculated results and field data are computed and applied to model results at each nodal point.

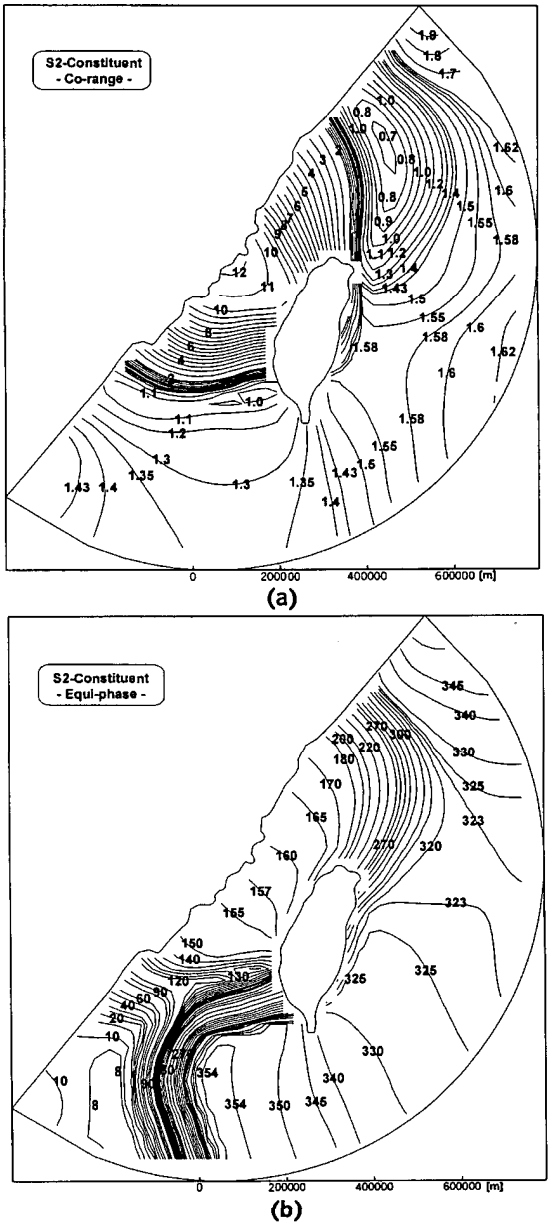

Fig. 8. Comparisons of computed amplitudes and phase-lags of S_2 constituent with incident angle of 180°. (a) and (b): computed co-range chart and equi-phase chart, (c) and (d): around the coast of Taiwan, (e) and (f): along part of the east coast of China.

6. Verifications of Computation Results with Field Data

6.1 Standing tides

In order to demonstrate the tidal characteristics shown in Figs. 3 and 4, a conceptual configuration of tides oscillating over a topographical shelf of specific width both in time and space domains is illustrated in Fig. 6.

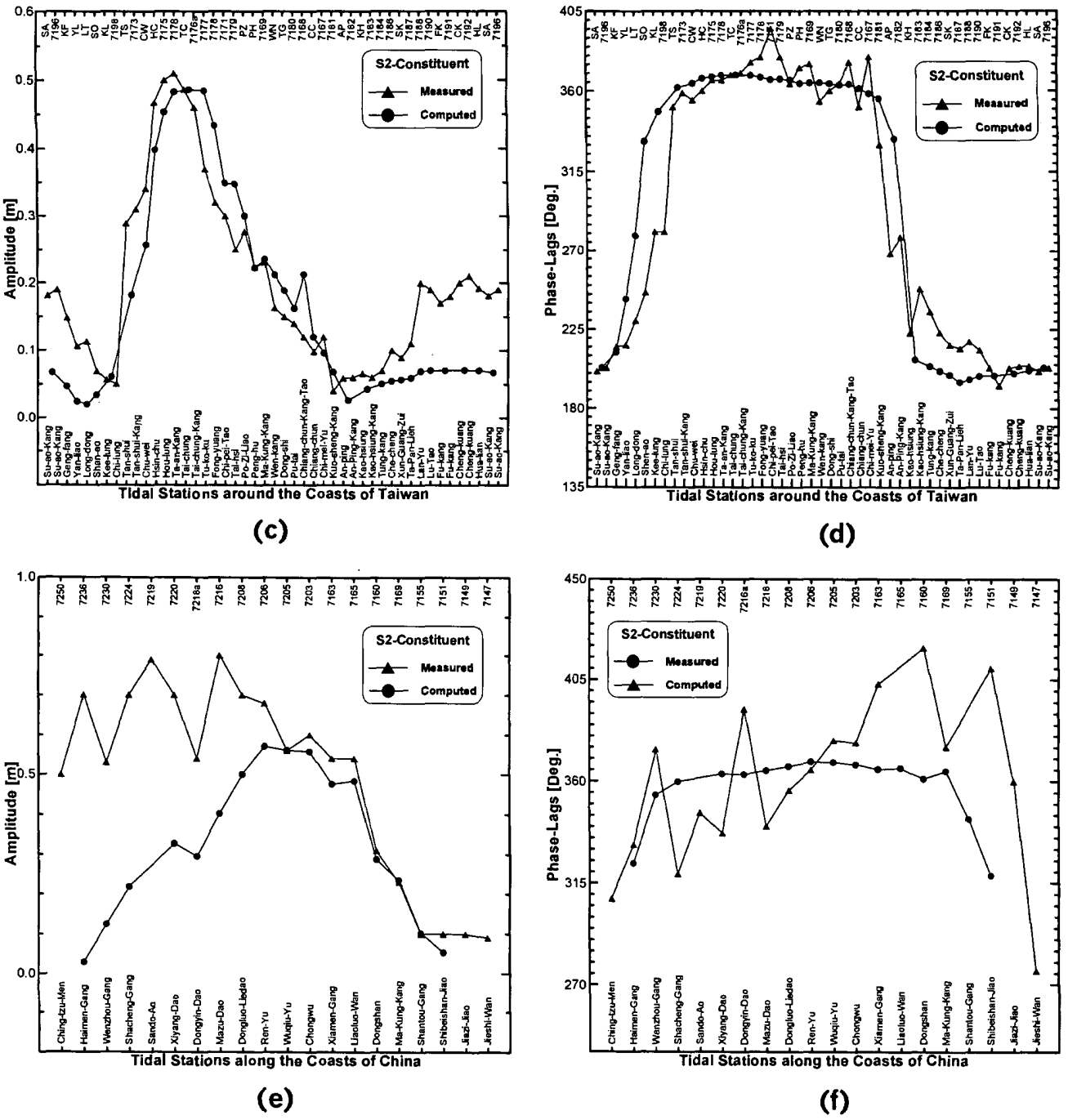

Fig. 8. (continued).

The symmetrical free surface displacements of a nearly standing tidal wave, $\eta(x,y;t)$, modulated in space and time domains, are described by

$$\eta(x,y;t) = \varsigma(x,y)\cos\left[\sigma t - \Theta\left(\vec{k}\cdot\vec{r}\right)\right], \tag{11}$$

where

$$\varsigma(x,y) = a\cos\left(\vec{k}\cdot\vec{r} - \pi/2\right), \tag{12}$$

and a denotes the amplitude of modulation, t denotes time, $\vec{k}$ represents the wave number vector, $\vec{r} = (x,y)$ denotes the position vector, $\Theta(\vec{k}\cdot\vec{r})$ denotes the phase-lag relative to the local high water time. It is observed from Fig. 3(b) that the distributions of phase-lags are symmetrically

distributed in space. They are approximately constant between stations Tan-shui and Chi-mei-yu, and decrease almost linearly beyond. From Eq. (12) with local origin of coordinates situated at one end of a continental shelf with width l, when $\vec{k} \cdot \vec{r} = (m + 1)\pi$ or $l = (m + 1)L/2$; $m = 0, 1, 2, 3, \ldots$, L denotes the wavelength of a specific tidal constituent, the tidal ranges will be approximately equal to zero at both shelf edges and will be largest at the central section of the shelf. For semidiurnal constituents in the Taiwan Strait of averaged water depth of 80 m, half of the characteristic wavelength, 625 km, will closely match the shelf width, 650 km, when $m = 0$. This fact implies that semidiurnal tidal waves are dominated by the standing oscillation in the Taiwan Strait.

The oscillations of free-surface displacement are demonstrated in Fig. 6 in terms of incremental time stages, namely $t = nT/24$; T is tidal period. The two stations near both nodes of the standing tide reach the time of high water simultaneously. As time progresses, i.e., n increases, these two high-water positions approach toward the central part of the shelf. The peculiar oscillation behavior looks like that there are two tidal waves propagating in opposite directions from both ends toward the middle point. This phenomenon, however, only indicates a spatially symmetrical modulation of tidal free surface oscillating in time domain. The correct propagating direction of specific constituent should be evaluated from the spatial gradient of equi-phase lines obtained in present numerical computations. On the other hand, simple wave encountering or standing waves fail to explain why the tidal ranges are much larger than the sum of heights of two oppositely propagating waves in the central west coast of Taiwan. From the symmetrical appearances of a nearly standing wave appear in a slender strait, the strait can be viewed as consisting of two finite-length channels with dead ends at the symmetrical point. With only one channel of specific length, Dean and Dalrymple (1984) have discussed that the co-oscillation resonance will be induced by a nearly standing wave with its node near to the entrance and anti-node at the dead end. Lin *et al.* (2000) have also concluded that a partially standing wave appears along the west coast of Taiwan, and the peculiar characteristics of tidal ranges resulted from resonance and wave trapped.

6.2 *The semidiurnal constituents*

From Figs. 3(a) and 4(a), it is noted that the M_2 constituent is the most dominant tide. The computed M_2 co-range and associated equi-phase chart is shown in Figs. 7(a) and (b), respectively. From the computed co-range chart, one can easily identify that a partially standing tidal wave exists in the Taiwan Strait. One node of the partially standing tide is located at the northeast coast near the Okinawa Trough, which is surrounded by the edge of the continent shelf and the Su-ao Ridge (Fig. 2). The other node is located at the southwest coast near the Kao-ping Slope, which is surrounded by the Taiwan Bank and the Heng-chun Ridge. From the equi-phase chart, the phase differences between these two nodes and station TC (the antinode) are close to 90°. Moreover, the phase angle of M_2 increases monotonically from 0° to 360° around the main island of Taiwan near station KH in clockwise sense. The distribution of phase angles remains perfectly in phase with itself after describing one complete circle. Although the Coriolis effects are neglected in present computation, however, present computed results are consistent with the description that trapped waves always propagate around an island in a clockwise sense in the north hemisphere (Louguet-Higgins, 1969).

With the computational results calibrated to the constituent harmonic constants of station TC, comparisons between measurements and computed results of amplitudes and phase-lags of M_2 constituent around the coast of Taiwan are shown in Figs. 7(c) and (d), respectively. It is noted that the maximum and averaged difference of computed amplitudes relative to observations is less than 0.31 and 0.14 m, respectively and the averaged difference of phase-lags is about 24°, or approximately 48 minutes. Good agreements of both the computed amplitudes and phase-lags are observed along the west coast of Taiwan and at the west offshore station Peng-hu (PH), except for the east stations from SA to SO and from SK to SA. It is worth pointing out that one of the computed nodes of the standing tide is located near station KH, in good agreement with data at the southwest coast of Taiwan. However, the other node is found on the northeast coast of Taiwan near station Fu-lung (FL), compared to the measured one at station SO. The southward shift of nodal position from SO to FL is not more than 20 km. From comparisons of the distributions of phase-lags, excellent agreements exist on most of the tidal stations except at the north coast from stations FL to KL. There are relatively large discrepancies in both amplitude and phase angle at the north coast of Taiwan. These discrepancies may be caused by neglecting the Coriolis effects or by the crude representation of local topography.

Comparisons of amplitudes and phase-lags of M_2 constituent along the east coast of China are shown in Figs. 7(e) and (f), respectively. It is noted that comparisons of amplitudes indicate good agreements from stations 7206 (Ren-yu) to 7155 (Jiazi-jiao), particularly, at station Wuqiu-yu (7205), an offshore islet. However, large discrepancies are found along the northeast coast stations from Haimen-gang (7236) to Dongluo-liedao (7208). It is observed by comparisons of phase-lags that large discrepancies appear along the southeast coast stations from Chongwu (7203) to Shibeishan-Jiao (7155). However, numerical results have the same general trend of distri-

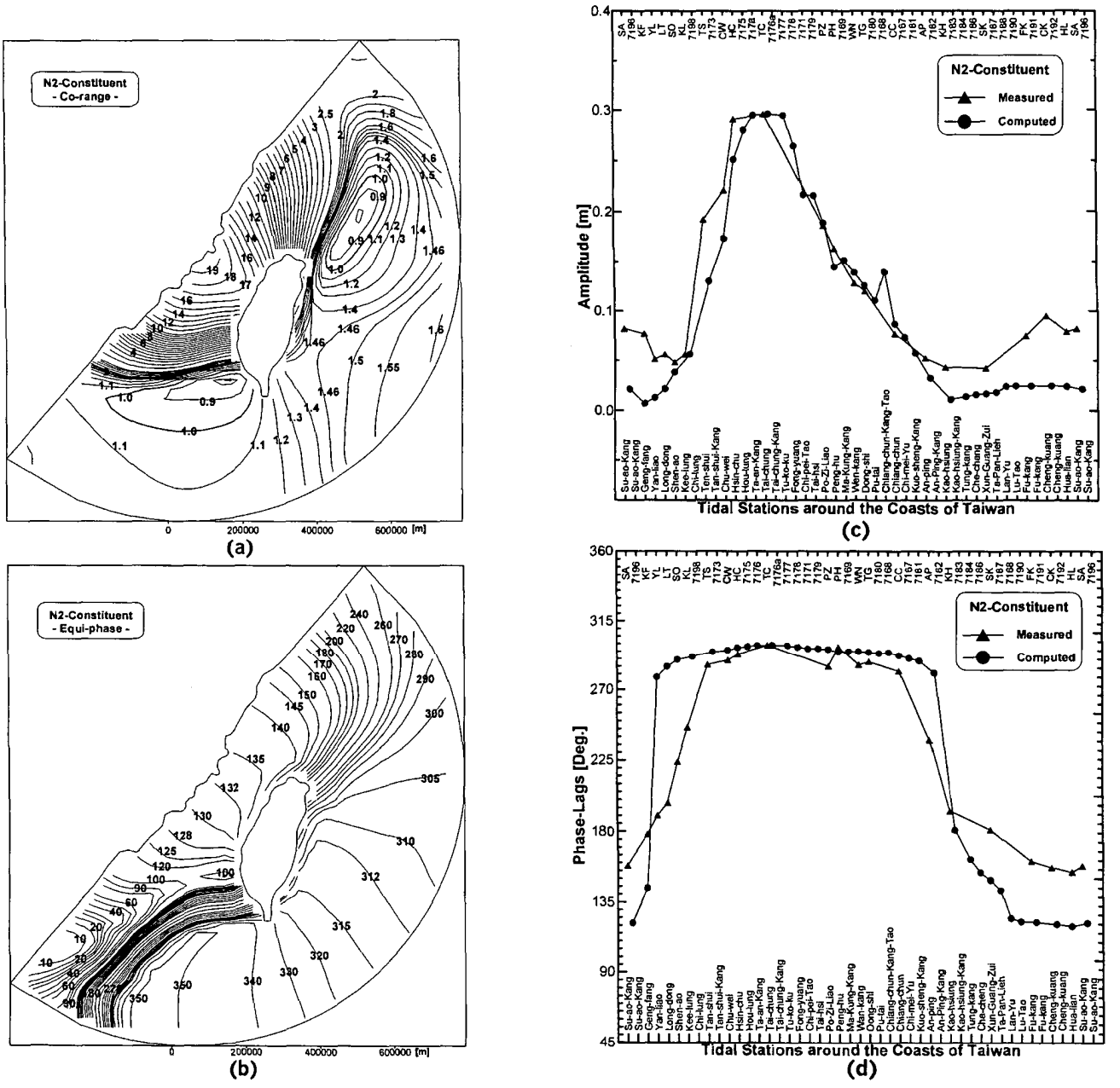

Fig. 9. Comparisons of computed amplitudes and phase-lags of N_2 constituent with incident angle of 180°. (a) and (b): computed co-range chart and equi-phase chart, (c) and (d): around the coast of Taiwan.

bution of amplitudes and phase-lags as the observations. The discrepancies may be due to the absence of Coriolis effects and inaccuracy of local topography and geometry in particular at locations close to both corner ends of China coast.

To further illustrate the characteristics of semidiurnal tides, two more numerical computations for S_2 and N_2 constituents are implemented. Their co-range and equi-phase charts with associated numerical results are shown in Figs. 8 and 9, respectively. Comparing the computational amplitudes and phase-lags with observed data around Taiwan, it is identified that the maximum difference of amplitudes is less than 0.13 m for S_2 and 0.07 m for N_2, and the averaged differences of phase-lags are about 18° for S_2 and 30° for N_2. Extremely good agreements are noted around the coasts of Taiwan. For future references, it is worth pointing out that the incident amplitudes of S_2, M_2, and N_2 are calibrated to be 0.045 m, 0.118 m, and 0.017 m, respectively.

The appearance of a nearly standing tide is also observed from the co-range and equi-phase charts, especially for N_2 constituent, Fig. 9(a). Lin *et al.* (2000) have described that maximum amplification appears in the Taiwan Strait when incident tide-period equals to 13.2 hours. All of semidiurnal tides thus fall into the band of resonance frequency. It is therefore anticipated that all semidiurnal amplitudes and phase-lags in Taiwan Strait will have similar distributions. From comparisons of amplitudes as well as phase-lags of constituents S_2 and N_2, good agreements are observed for tidal stations around the coast of Taiwan. For tidal distributions along the east coast of China, similar trends of discrepancies occur as those of M_2 constituent.

6.3 The diurnal constituents

Tidal computations of diurnal constituents: K_1, O_1, and P_1 are also implemented for reference of model verification, even though the Coriolis effects can no longer be negligible. Since the computed results of these three diurnal constituents show similar characteristics, only the computed co-range and equi-phase charts associated with comparisons of the amplitudes and phase-lags of K_1 constituent are shown in Fig. 10. It is clear that diurnal tidal waves are propagating in the direction from north to south even though the incident angle is 180° (from east to west). The configuration of partially standing tides, which appears in semidiurnal constituents, is no longer observed. It is interesting to note that high accuracy of the computed amplitudes with averaged discrepancies not more than 2.5 cm are achieved both around the coast of Taiwan and along the coast of China. However, the trend of distributions of phase-lags is not captured in these computations, even though the maximum discrepancies are generally no more than 45°.

7. Conclusions

The tidal characteristics in Taiwan Strait are demonstrated in this paper. Based on the shallow-water wave equation which can be reduced from the mild-slope equation with neglect of Coriolis force, numerical investigations on anomalous amplification of semidiurnal tides in the Taiwan Strait are performed. From both field data and computed results, it is noted that the distributions of tidal amplitudes are more symmetric for semidiurnal tides than for diurnal ones. The ranges of semidiurnal amplitudes along the China coast also are larger than those around the coast of Taiwan. The fact that the length of Taiwan Strait nearly equals to half wavelength of semidiurnal tides significantly affects the tidal behaviors in this area. Results of the present model demonstrate in good accordance with field measurements for semidiurnal tides around the coast of Taiwan. The averaged difference of computed phase-lag is about 24° (18° of S_2, 24° of M_2, and 30° of N_2), or approximately 0.8 hours. The largest differences of amplitudes are less than 0.31 m in all semidiurnal cases. Because the referenced point of calibration is chosen at station TC, the stations with larger differences typically occur along the east coast of Taiwan. On the other hand, the computed amplitudes and phase-lags along the coast of China can fit the observation only along central half flank.

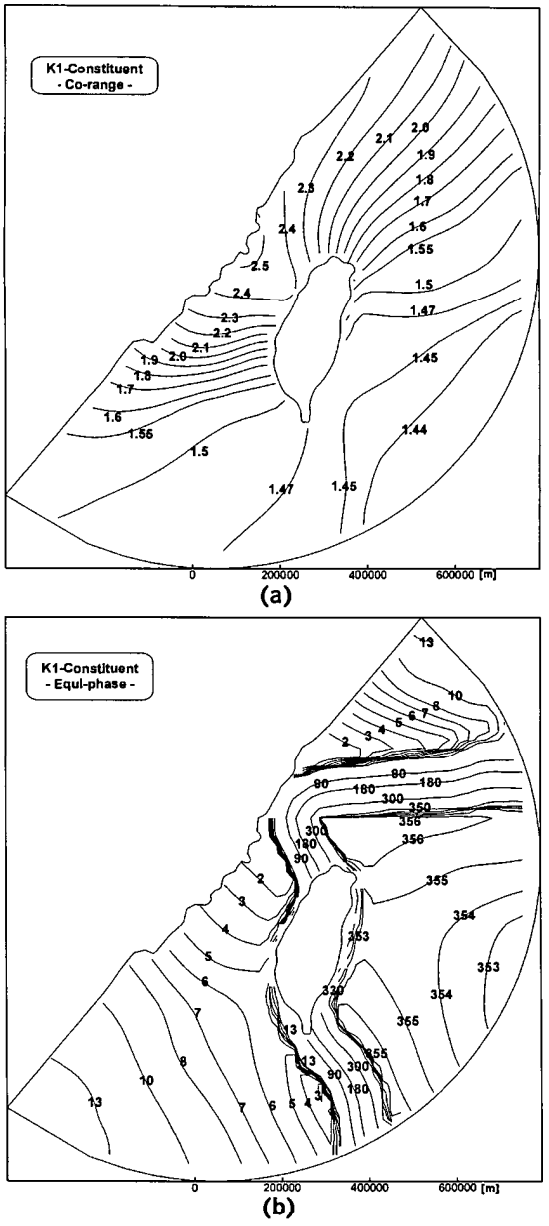

Fig. 10. Comparisons of computed amplitudes and phase-lags of K_1 constituent with incident angle of 180°. (a) and (b): computed co-range chart and equi-phase chart, (c) and (d): around the coast of Taiwan, (e) and (f): along part of the east coast of China.

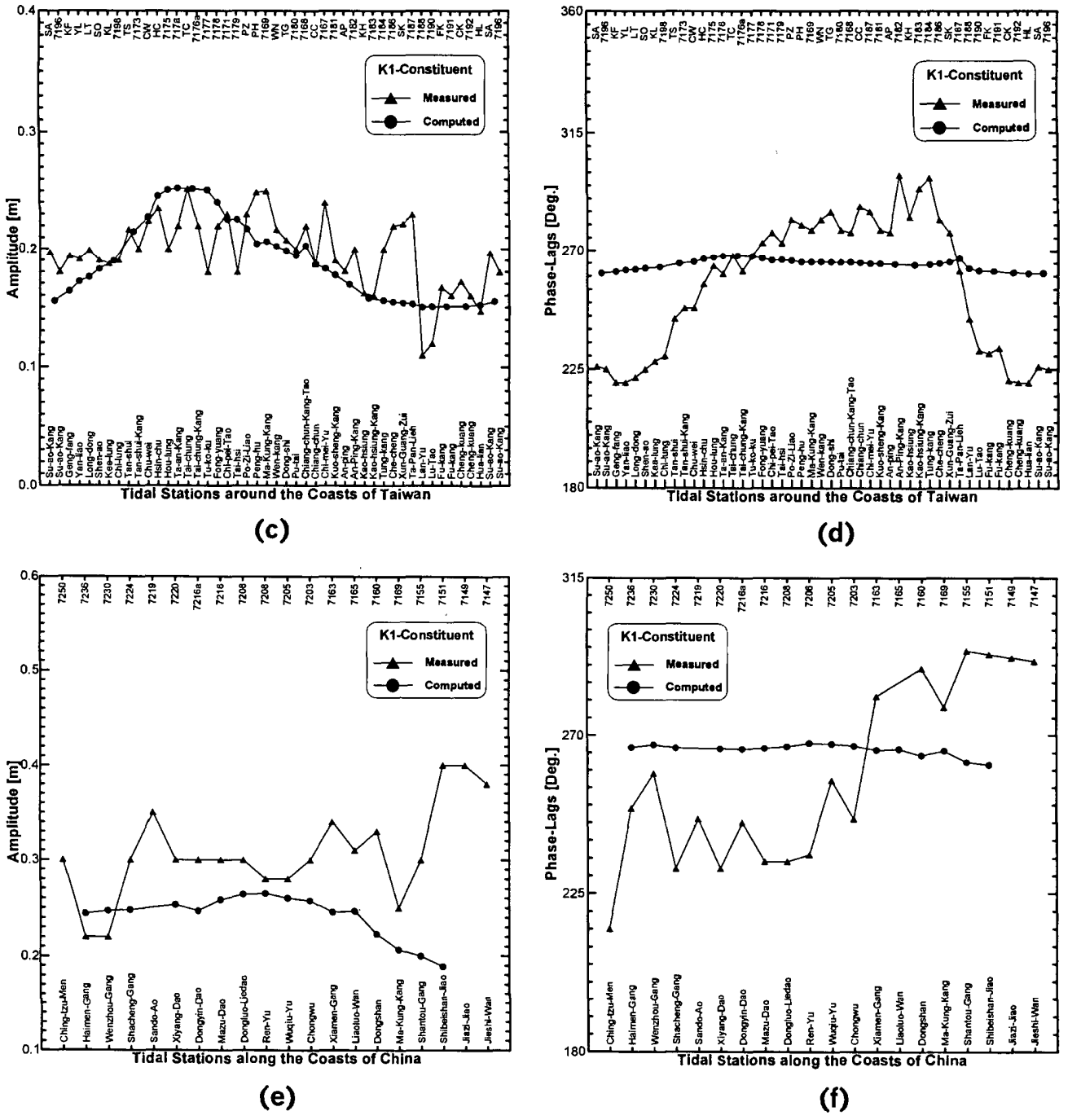

Fig. 10. (continued).

Based on the comparisons between observed data and model results, the 2-D long-wave approximation of the mild-slope equation with neglect of Coriolis force has been successfully extended to compute the transformation behaviors of semidiurnal tides in the Taiwan Strait. The present numerical model is linear and of energy-conserving type in frequency domain. The calibration of present computed results requires only incident tidal wave amplitude and propagation angle. It implies that energy dissipation is not important. The present model also has advantage over transient tidal computations in which model applicability is dependent on accuracy of the open boundary conditions.

Acknowledgements

The authors would like to express their sincere thanks to Mr. Wen-Jiunn Liou, senior specialist of Central Weather Bureau, Taiwan, for his kind provision of tidal field measurement. Gratitudes also go to our colleagues: Dr. Jinn-Hwa Shyu, researcher, and Mr. Chung-Chiuan Chiang, assistant researcher, Institute of Harbour and Marine Technology, for their encouraging and fruitful discussions. The third author would like to express his gratitudes for financial support from National Science Council of Taiwan under contracts of NSC-86-2621-D-002-019, NSC-87-2621-D-002-060, and NSC-88-2611-E-002-032. Comments and suggestions from Professors John Wang, University of Miami, and Dong-Ping Wang, State University of New York at Stony Brook, are highly appreciated.

References

Berkhoff, J. C. W. (1972): Computation of combined refraction-diffraction. *Proc. of the 13th Int. Conf. Coastal Eng.*, Vancouver, British Columbia, Canada, p. 471–490.

Booij, N. (1983): A note on the accuracy of the mild-slope equation. *Coastal Eng.*, **7**, 191–203.

Cartwright, D. E. (1990): Oceanic tides from geosat altimetry. *J. Geophys. Res.*, **95**, C3, 3069–3090.

Chapman, D. C. (1985): Numerical treatment of cross-shelf boundaries in a barotropic coastal ocean model. *J. Phys. Oceanogr.*, **15**, 1060–1075.

Chen, B. S. and T. K. Tsay (1990): Application of local radiation condition to water-wave numerical modeling. *Proc. 12th Conf. on Ocean Eng.*, CICHE, p. 1–18 (in Chinese).

Chen, H. S. and C. C. Mei (1974): *Oscillations and Wave Forces in a Man-Made Harbor in the Open Sea.* TR No. 190, Ralph M. Parsons Lab., Dept. Civil Engrg., MIT.

Copeland, G. J. M. (1985): A practical alternative to the mild-slope wave equation. *Coastal Eng.*, **9**, 125–149.

Dean, R. G. and R. A. Dalrymple (1984): *Water Wave Mechanics for Engineers and Scientists.* Chapter 5, Prentice-Hall, Englewood Cliffs, New Jersey, 353 pp.

Egbert, G. D., A. F. Bennett and M. G. G. Foreman (1994): TOPEX/POSEIDON tides estimated using a global inverse method. *J. Geophys. Res.*, **99**, C12, 24821–24852.

Guo, X. and T. Yanagi (1998): Three-dimensional structure of tidal current in the East China Sea and the Yellow Sea. *J. Oceanogr.*, **54**, 651–668.

Kirby, J. T. (1986): A general wave equation for waves over rippled beds. *J. Fluid Mech.*, **162**, 171–186.

Le Provost, C., M. L. Genco and F. Lyard (1994): Spectroscopy of the world ocean tides from a finite element hydrodynamic model. *J. Geophys. Res.*, **99**, C12, 24777–24797.

Lin, M. C., W. J. Juang and T. K. Tsay (2000): Anomalous amplification of semidiurnal tides along the west coast of Taiwan. *Ocean Engineering* (to appear).

Liu, S. K. (1984): *A Three Dimensional Model of the China Seas.* The Science and Technology Advisory Group, The Executive Yuan, R.O.C.

Louguet-Higgins, M. S. (1968): On the trapping of wave along a discontinuity of depth in a rotating ocean. *J. Fluid Mech.*, **31**, 417–434.

Louguet-Higgins, M. S. (1969): On the trapping of long-period waves round islands. *J. Fluid Mech.*, **37**, 773–784.

Lynch, D. R. and C. E. Naimie (1993): The M_2 tide and its residual on the outer banks of the Gulf of Maine. *J. Phys. Oceanogr.*, **23**, 2222–2253.

Madsen, P. A. and J. Larsen (1987): An efficient finite-difference approach to the mild-slope equation. *Coastal Eng.*, **11**, 329–351.

Mei, C. C. (1983): *The Applied Dynamics of Ocean Surface Waves.* Chapter 6, Wiley, New York, 740 pp.

Schureman, P. (1988): *Manual of Harmonic Analysis and Prediction of Tides.* Coast and Geodetic Survey, U.S. Department of Commerce, U.S. Government Printing Office, Washington, D.C., 317 pp.

Smith, R. and T. Sprinks (1975): Scattering of surface waves by a conical island. *J. Fluid Mech.*, **72**, 373–384.

Tsay, T. K. (1991): Linear surface waves over rotating fluids. *J. Waterway, Port, Coastal, and Ocean Eng.*, **117**, 2, 156–171.

Tsay, T. K., W. Zhu and P. L.-F. Liu (1989): A finite element model for wave refraction, diffraction, reflection and dissipation. *J. Applied Ocean Res.*, **11**, 33–38.

UK Hydrographic Office (UKHO) (1997): *Admiralty TIDE TABLES and Tidal Stream Tables.* Vol. 3, The Hydrographer of the Navy, Somerset, U.K., 498 pp.

Wagner, C. A., C. K. Tai and J. M. Kuhn (1994): Improved M_2 ocean tide from TOPEX/POSEIDON and Geosat altimetry. *J. Geophys. Res.*, **99**, C12, 24853–24865.

Wang, D. P. (1982): Development of a three-dimentional, limited-area (island) shelf circulation model. *J. Phys. Oceanogr.*, **12**, 605–617.

Yanagi, T., T. Takao and A. Morimoto (1997): Co-tidal and co-range charts in the South China Sea derived from satellite altimetry data. *La mer*, **35**, 85–93.

Zahel, W. (1991): Modeling ocean tides with and without assimilating data. *J. Geophys. Res.*, **96**, B12, 20379–20391.